Topological and superconducting properties in YD_3 (D = In, Sn, Tl, Pb)

Xin-Hai Tu,[1,2,3] Peng-Fei Liu,[1,2] and Bao-Tian Wang[1,2,4,5,*]

[1]*Institute of High Energy Physics, Chinese Academy of Sciences (CAS), Beijing 100049, China*

[2]*Dongguan Neutron Science Center, Dongguan 523803, China*

[3]*University of Chinese Academy of Sciences, Beijing 100039, China*

[4]*Institute of Applied Physics and Computational Mathematics, Beijing 100088, China*

[5]*Collaborative Innovation Center of Extreme Optics, Shanxi University, Taiyuan, Shanxi 030006, China*

(Received 24 January 2019; revised manuscript received 23 March 2019; published 13 May 2019)

Using first-principles calculations, we explore the electron properties of YD_3 (D = In, Sn, Tl, Pb) and predict that YIn_3, YTl_3, and YPb_3 are topological superconductor candidates. In the presence of spin-orbit coupling effect, continuous band gaps for YIn_3, YSn_3, and YPb_3 are opened between their highest occupied bands (N) and the lowest unoccupied bands ($N+1$), where the different Z_2 invariants are obtained. Differently and specially, there are type-II Dirac points (DPs) at the high-symmetry lines in YTl_3, indicating one possibility of topological Dirac semimetal. Furthermore, the nontrivial Rashba-like topological surface states are achieved at the $\bar{X}$ point on the (001) surface for YIn_3, YTl_3, and YPb_3, as well as the Fermi arcs in YTl_3 connecting the DPs. In addition to the topological properties, our electron-phonon coupling calculations indicate clearly that these four intermetallics are all phonon-mediated superconductors. The calculated superconducting transition temperatures of T_c = 0.96, 6.34, 2.17, and 4.37 K respectively for YIn_3, YSn_3, YPb_3, and YTl_3 agree well with experiments.

DOI: 10.1103/PhysRevMaterials.3.054202

I. INTRODUCTION

Topological materials have attracted much attention after the quantum spin Hall state (QSHS) being proposed theoretically [1–3] and revealed in the HgTe quantum wells [4] experimentally. These materials can be detected the nontrivial topological surface states (TSSs) protected by the symmetry of their bulk. For example, topological insulators (TIs) [5–10] have gapped band structures in bulk around the Fermi level but gapless TSSs at surface protected by time-reversal symmetry. Same as the Chern number defined in the whole two-dimensional (2D) Brillouin zone (BZ) for three-dimensional (3D) insulators, the topological invariants in 3D metals can also be defined on a closed 2D manifold, such as the Fermi surface [11].

To date, topological semimetals (TSMs) and topological superconductors (TSs) have been suggested to extensively possess potential applications in transport [12–15] and topological quantum computation [9,16–19]. TSMs [13,20,21] have band crossings at the Fermi level, such as DPs protected by additional crystal symmetry in bulk, and the nontrivial TSSs with Fermi arcs [22,23]. Different from Dirac semimetals, Weyl semimetals [24–26] have paired Weyl points with opposite chirality. Breaking time-reversal or inversion symmetry lifts the Kramers degeneracy of bands. Hence a pairwise crossing of bands leads to a twofold instead of a fourfold degeneracy. These twofold degeneracy points are protected and topologically stable against any perturbation. To annihilate a pair of Weyl points with opposite chirality, the only way is to move them to the same point in BZ. In nodal line semimetals [21,27,28], the cross points constitute a line or a closed curve, and the drumheadlike TSSs can be observed at the surface. TSs [9,29–32] are distinguished by a superconducting gap in bulk and Majorana fermions, a sort of exceptional quasiparticle that is its own antiparticle and obeys non-Abelian statistics, at boundary. Theoretically, a spinless $p+ip$ type superconductor can hold Majorana zero modes at the vortices. The previous work by Fu *et al*. [7,9,33] has proposed that the topological superconductivity can be realized on the interface between a TI and a Bardeen-Cooper-Schrieffer (BCS) superconductor. Very recently, Zhang *et al*. [34] proposed a kind of single-compound TS candidate β-$RhPb_2$ that has nontrivial spin-helical TSSs. The superconductivity in TSMs and the corresponding interpretation [35–37] have also been proposed in Cd_3As_2 [38], $PbTe_2$ [39], and $MoTe_2$ [40]. These inspire us to explore topological features in superconductors.

AG_3 (A = La, Y; G = Sn, In, Pb, Tl) compounds [41–46], crystallized in the $AuCu_3$-type cubic structure, have been explored extensively and intensively. Much interest in these systems is due to their abundantly physical phenomena, such as superconductivity, heavy fermion behavior, and other novel quantum properties [45–48]. The superconducting transition temperature T_c = 6.25 and 7.0 K for $LaSn_3$ and YSn_3, repectively, are higher than $LaIn_3$ and YIn_3 that were reported with T_c lower than 1.0 K [43,49]. Other compounds, for instance, $PrSn_3$ and $NdSn_3$, hold antiferromagnetic order at the Néel temperatures T_N of 8.6 and 4.5 K [50], respectively. $CeSn_3$, exhibiting valence fluctuations, has been categorized as a dense Kondo compound [51]. A few years ago, Ram *et al*.

*Author to whom correspondence should be addressed: wangbt@ihep.ac.cn

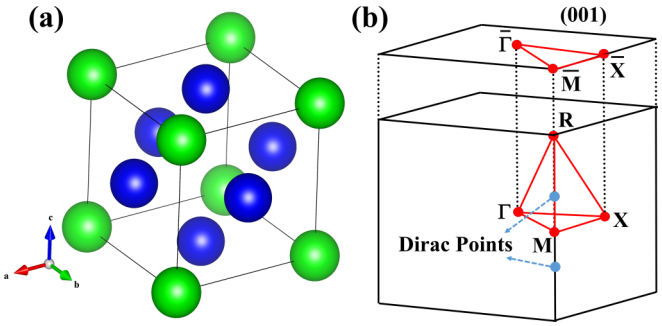

FIG. 1. Lattice structure (a) and BZ (b) of YD_3. The green and blue balls represent Y and D atoms, respectively. The red lines mark out the high-symmetry paths for the bulk and the (001) surface. The blue solid circles show the locations of the DPs in YTl_3.

[52] systematically studied the Fermi surface properties of AG_3 (A = La, Y; G = Sn, In, Pb, Tl) intermetallics under pressure.

In the present work, we propose that the $AuCu_3$-type intermetallics of YIn_3, YTl_3, and YPb_3 are not only superconductors [53] but also topological materials. When considering spin-orbit coupling (SOC) effect, by the evidences of the band inversions and the nontrivial Z_2 invariants as well as the Rashba-like gapless TSSs on the (001) surface, the nontrivial topological properties are inferred to exist. On the basis of full gaps between N and $N+1$ bands, the Z_2 indices as (0; 111) and (1; 111) are calculated for YIn_3 and YPb_3, respectively. For YTl_3, according to crystal symmetry, there are 24 type-II DPs with fourfold degeneracy at the high-symmetry lines. The Fermi arcs linking two DPs are also observed at surface. For YSn_3, it is a topologically trivial system. This paper is organized as follows. First, we introduce the details of crystal structure and first-principles calculations in Sec. II. Next, in Sec. III, the calculation results are presented. Finally, Sec. IV contains the discussion and conclusion.

II. CRYSTAL STRUCTURE AND COMPUTATIONAL DETAILS

The face centered cubic structure of YD_3 with space group of $Pm\bar{3}m$ (No. 221) and holding apparent inversion symmetry are shown in Fig. 1(a). Figure 1(b) displays the corresponding BZ and the high-symmetry paths for electron and phonon-related calculations. To investigate the electronic structures, phonon spectra, and electron-phonon coupling (EPC), the first-principles calculations are performed using the QUANTUM ESPRESSO package [54] based on the density functional theory [55,56] and the density functional perturbation theory [57]. The generalized gradient approximation of Perdew-Burke-Ernzerhof [58] type and the projector augmented wave potentials are used for interactions between electrons and nuclei [59,60]. An unshifted $18 \times 18 \times 18$ **k**-point mesh are adopted in the 3D BZ. The kinetic-energy cutoffs of the plane wave expansion are 60, 75, 80, and 50 Ry, and the energy cutoffs for charge density are 480, 600, 640, and 400 Ry for YIn_3, YSn_3, YTl_3, and YPb_3, respectively. The optimized lattice constants are $a = 4.709$, 4.729, 4.809, and 4.899 Å, respectively, closing to experimental values [49,61]. In the electronic structure calculations, the full relativistic pseudopotentials are employed when taking the SOC effect into account. In calculating the phonon dispersions with a $6 \times 6 \times 6$ **q** mesh, since the effect of SOC is less important in describing the vibrational properties [62–66], we neglect this effect. The maximally localized Wannier functions for all Y d and D sp orbitals are generated to construct the tight-binding Hamiltonians. With the help of WannierTools codes [67], we calculate the TSSs, Fermi surfaces, and spin textures.

III. DETAILS OF RESULTS

A. Band structures and topological invariants

The orbital-resolved band structures of YD_3 with SOC effect are plotted along the high-symmetry path in

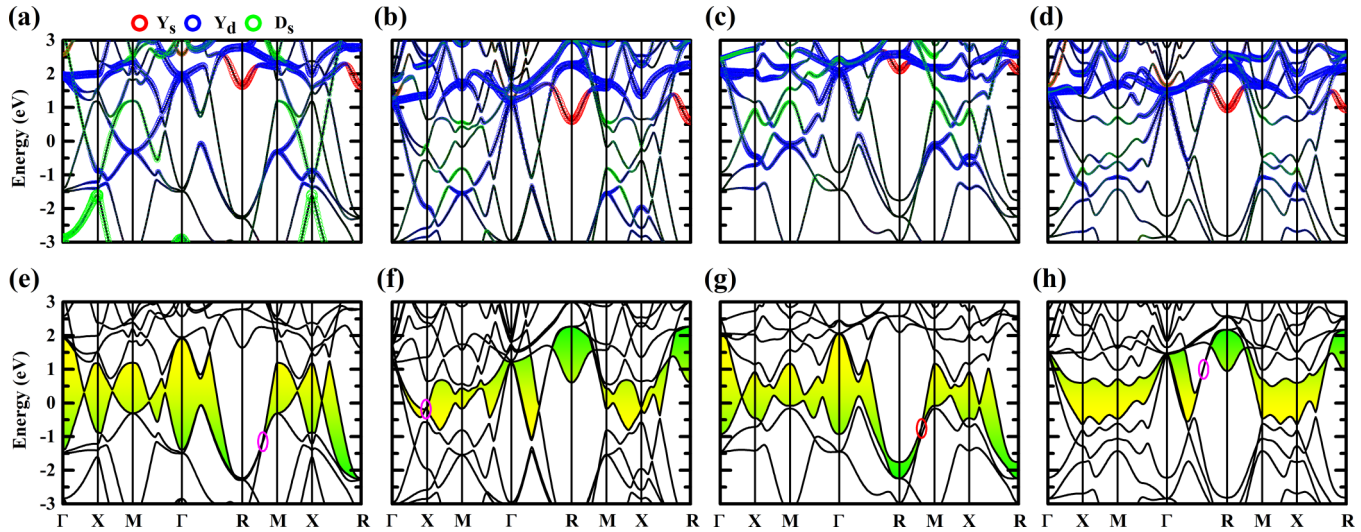

FIG. 2. Orbital-resolved band structures with SOC effect of YIn_3 (a), (e), YSn_3 (b), (f), YTl_3(c), (g), and YPb_3 (d), (h). (a)–(d) The red, blue, and green bubbles represent the contributions of Y s, Y d, and D s orbitals, respectively. (e)–(h) The continuous band gaps between N and $N+1$ bands are daubed by yellow-green color. The DP in YTl_3 and the locations of the narrowest band gaps in three other materials are highlighted by the ellipses.

TABLE I. Parity products at TRIMs and the Z_2 indices of YD_3.

	YIn_3	YSn_3	YTl_3	YPb_3
TRIMs		Parity products		
Γ	+	+	+	+
$X \times 3$	−	−	−	+
$M \times 3$	−	+	−	+
R	+	−	+	−
Plane ($i = x, y, z$)		Z_2 values		
$k_i = 0$	1	0	1	0
$k_i = \pi$	1	0	1	1
$(\nu_0; \nu_1\nu_2\nu_3)$	(0; 111)	(0; 000)	(0; 111)	(1; 111)

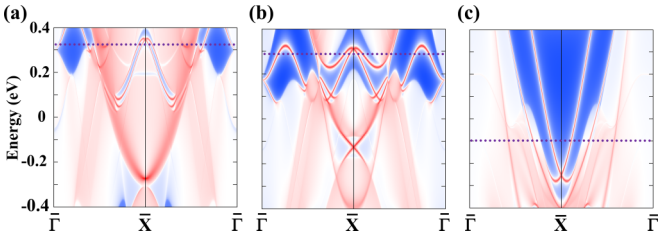

FIG. 3. Bright-colored red lines mean the TSSs on the (001) surface of YIn_3 (a), YTl_3 (b), and YPb_3 (c). The purple dotted lines show the chemical potentials at the energy levels of $E - E_F = +0.325$, $+0.29$, and -0.10 eV for depicting Fermi surfaces of YIn_3, YTl_3, and YPb_3, respectively.

Figs. 2(a)–2(d). Around the Fermi level (±3 eV), the D p (In, Sn 5p; Tl, Pb 6p) orbitals (not shown in Fig. 2) dominate the bands and spread over the whole BZ while the contributions from the Y 4s4d and D s (In, Sn 5s; Tl, Pb 6s) orbitals are not that visible. In the vicinity of energy level at 2 eV, the Y 4d orbital is predominant and the Y 4s orbital can only be found near the R point. One can discover clearly that there are band inversions [13,28,68], a remarkable signal for topological materials, induced by Y d and In (Tl) s orbitals around the M point in YIn_3 (YTl_3). Nevertheless, in YSn_3 and YPb_3, the band inversions are caused by Y d and Y s orbitals around the R point.

Since time-reversal and inversion symmetries can lead to spin degenerate bands, the tilted band crossing between the N and $N + 1$ bands below the Fermi level about 0.7557 eV at (0.5,0.5,0.19) [red ellipse in Fig. 2(g)] and along the R-M direction for YTl_3 is fourfold degeneracy. Actually, we checked the magnetic moments of these four systems. The d orbitals of Y atoms don't introduce local magnetic moments in the cell so ensuring the time-reversal symmetry. In terms of crystal symmetry, there are a total of 24 type-II DPs in BZ and each of them is protected by C_4 rotational symmetry. If the time-reversal or inversion symmetry is broken, one DP will split into two Weyl points, and the crossings will move away from the high-symmetry lines. Also, if conserving time-reversal and inversion symmetries but breaking C_4 rotational symmetry or doping electrons/holes to gap out the DPs, we can get a TI-like material. Thus the nontrivial Z_2 indices (0; 111), as shown in Table I, can be calculated via parity criterion [69,70] because of the existence of inversion symmetry.

The eight time-reversal invariant momentum points (TRIMs) in 3D BZ are defined as $\Gamma_{n_1,n_2,n_3} = \frac{1}{2}(n_1\mathbf{G}_1 + n_2\mathbf{G}_2 + n_3\mathbf{G}_3)$, where $n_{1,2,3} = 0$ or 1 and $\mathbf{G}_{1,2,3}$ are the primitive reciprocal lattice vectors. Then we can calculate the strong topological index ν_0 by $(-1)^{\nu_0} = \prod_{i=1}^{8} \delta(\Gamma_i)$, where $\delta(\Gamma_i)$ is the product of parity eigenvalues of the occupied bands below the gap at the TRIM Γ_i. The weak topological indices $\nu_{1,2,3}$ are defined as the products of parity eigenvalues of four TRIMs in a plane ($\mathbf{k}_{x,y,z} = \pi$) offset from the Γ point.

Different with YTl_3, as marked by the yellow-green color in Figs. 2(e), 2(f), and 2(h), there are continuous band gaps between N and $N + 1$ bands for the other three materials on which we focused. The narrowest gaps, highlighted by the pink ellipses, are 35, 1, and 5 meV at (0.5, 0.5, 0.25), (0.32, 0.0, 0.0), and (0.31, 0.31, 0.31) for YIn_3, YSn_3, and YPb_3, respectively. Because such a global SOC gap exists in the whole BZ, the topological Z_2 invariants can be defined. In Table I, we show the parity eigenvalues at eight TRIMs and give the Z_2 indices $(\nu_0; \nu_1\nu_2\nu_3)$ as (0; 111), (0; 000), and (1; 111) for YIn_3, YSn_3, and YPb_3, respectively. It is clear that YPb_3 is a strong topological material but YSn_3 isn't and YIn_3 is a weak topological material. Supposing that a plane has nontrivial Z_2 indices, the QSHS can be revealed on that plane. A Kramers pair of surface states connecting valence and conduction states has to appear in the gap in this case [24]. Therefore, we can obtain TSSs on the (001) surface, which will be discussed at the next section. For details, in Table II, we show the parity eigenvalues of each occupied band at TRIMs for the four systems.

B. Surface states and Fermi surfaces

In addition to Z_2 invariants, the existence of TSSs is another prominent hallmark of topological materials. Fortunately, even though the fully gapped bands (as shown in Fig. 2) are weird and unsatisfactory, the TSSs (as shown in Fig. 3) are not overlapped and distinguished obviously from the bulk bands on the (001) surface for YIn_3, YTl_3, and YPb_3. The Rashba-like TSSs protected by time-reversal symmetry, closing the bulk band, are observed at the $\bar{X}$ point around 0.3 eV for YIn_3 and YTl_3, but -0.3 eV for YPb_3. Note that the crossing around -0.1 eV at the $\bar{X}$ point in YTl_3, reflecting the properties between $N - 1$ and N bands, is out of the scope of our present work. Another mentionable thing is that the TSS in YPb_3 crosses over the Fermi level. This feature can contribute to its transport properties and will be observed easily in angle-resolved photoemission spectroscopy (ARPES) experiments [34]. Figure 4 shows the Fermi surfaces at the chemical potentials of 0.325, 0.29, and -0.1 eV, as highlighted by the purple dotted lines in Fig. 3, and corresponding spin textures for YIn_3, YTl_3, and YPb_3, respectively. Once YIn_3 and YPb_3 become superconductors below superconducting temperature, the TSSs around the $\bar{X}$ point will be guided into superconducting phase by the proximity effect and possess the equivalent $p + ip$ type superconductivity [31,33].

Besides the closed Fermi surfaces (Fig. 4), the disconnected open Fermi arcs, lines that originate and terminate at the same DP or connect two different DPs together [20], can give rise to the edge modes of the QSHS [24]. Theoretically, there are twelve projected DPs (green solid circles) at (±0.5,

TABLE II. Parity eigenvalues of 25 (27) occupied bands at eight TRIMs of YIn_3 and YTl_3 (YSn_3 and YPb_3).

TRIMs	YIn_3	YSn_3	YTl_3	YPb_3
Γ	+ − − − + + + +	+ − − − + + + + +	+ − − − + + + +	+ − − − + + + + +
	+ + + + + + + +	+ + + + + + + + +	+ + + + + + + +	+ + + + + + + + +
	+ + + + + + − − −	+ + + + − − − + +	+ + + + + + − − −	+ + + + − − − + +
$X \times 3$	+ − − − − − + +	+ − − − − − + + −	+ − − − − + − +	+ − − − − + − + −
	− − − − + + − +	− − − + + − + − −	− − − − − + + +	− − − + − + + − −
	− − − − + + − + +	− − + + − + + − −	− − − − + − + + +	− − + − + + + + −
$M \times 3$	+ − − − − − + −	+ − − − − − + − +	+ − − − − − + +	+ − − − − + − − +
	+ − − − + + − −	− − − + + − − + −	− − − − + − + −	− − − + + − − + −
	+ − − + − − + + +	− + − − + + + + −	+ − − + − − + + +	− + − − + + + + −
R	+ − − − + + + +	+ − − − + + + + +	+ − − − + + + +	+ − − − + + + + +
	+ + + + + + + +	+ + + + + + + + +	+ + + + + + + +	+ + + + + + + + +
	+ + + + + + − − −	+ + + + − − − − +	+ + + + + − −	+ + + + − − − − +
Products	+ − − +	+ − + −	+ − − +	+ + + −

±0.19), (±0.19, ±0.5), and (±0.5, ±0.5) on the (001) surface in YTl_3, as shown in Fig. 5. Owing to the interference of the bulk bands along the X-M and the R-M directions, the DPs are hidden, which results in difficult observation of the Fermi arcs. Even so, we could find clearly the ropelike Fermi arcs connecting two DPs in Fig. 5(b). A previous work [71] discussed that the Fermi arcs on Dirac semimetal surface are not topologically protected, unlike the Fermi arcs in Weyl semimetals, and can be continuously deformed into a closed Fermi contour by a small bulk perturbation.

C. Phonon dispersions and superconductivity

In this section, we focus on the conclusions of the EPC properties in YD_3 (see the Supplemental Material [72] for more details). As we can see from the purely positive phonon spectra (Fig. S1), these four materials are all dynamically stable. To enhance the total EPC, one can see from the phonon spectra weighted by the EPC λ_{qv} that the soft phonon modes make critical contributions. Furthermore, combining the phonon dispersions weighted by the atomic vibrations as well as by the EPC λ_{qv}, we can find that the main contribution to the EPC is from the D atoms at Cu sites, whereas the Y atoms only make limited contributions to the EPC. Finally, the superconducting transition temperature of $T_c = 0.96$, 6.34, 2.17, and 4.37 K, respectively for YIn_3, YSn_3, YTl_3, and YPb_3, are very close to the experimental values of $T_c = 0.78$, 7, 1.52, and 4.72 K [49,61], and also in good accordance with one recent DFT result [53]. This indicates that our results are reliable and all the YD_3 systems are phonon-mediated superconductors.

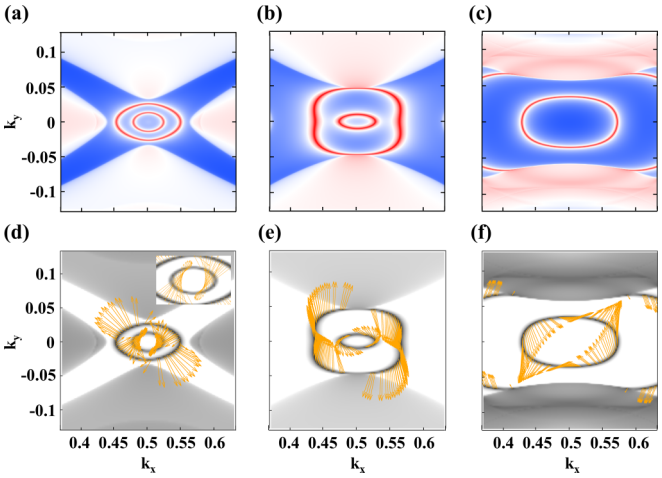

FIG. 4. Fermi surfaces and corresponding spin textures of YIn_3 (a), (d), YTl_3 (b), (e), and YPb_3 (c), (f) at the chemical potential of 0.325, 0.29, and −0.1 eV, respectively. The yellow arrows mean the directions of spin at TSSs.

IV. DISCUSSION AND CONCLUSION

Some previous proposals of TS candidates, such as Cu/Nb-doped Bi_2Se_3 [73,74], In-doped SnTe [75], β-$RhPb_2$ [34], and $TaSe_3$ [76], have been theoretically predicted or experimentally verified. Searching for intrinsic TSs, introducing superconductivity by doping in TIs or adding pressure, and building heterostructures by TIs and superconductors are the major approaches to realize topological superconductivity in real materials. Recently, superconductivity has also been observed in TSMs $PdTe_2$ [39,77], $MoTe_2$ [40], and YPtBi

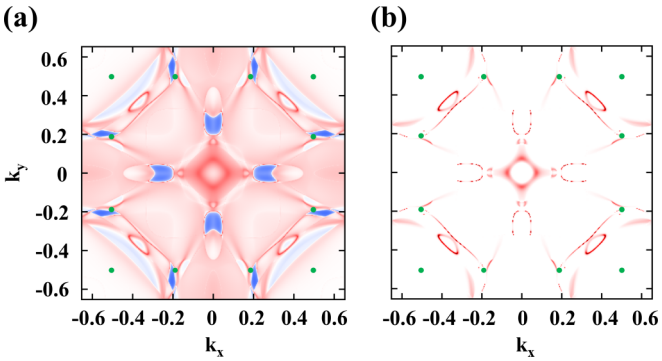

FIG. 5. (a) Fermi surface of YTl_3 at a chemical potential of −0.7557 eV where the DPs (green circle) are located. (b) The Fermi surface filtered out the bulk bands.

[78]. Hashimoto *et al*. [39] proposed that the orbit-momentum locking is the key in TSMs to interpret the superconducting gap structure of the possible superconducting state.

Here we show theoretically that three promising candidates of YIn_3, YTl_3, and YPb_3, whose superconductivity and other interesting physical properties have been reported for many years, are topologically nontrivial. Compared to the above reported TS candidates, these three systems have simple $AuCu_3$-type cubic structure that avoids the effect of impurity, disorder, and distortion caused by doping. Along the X-M path, the SOC effect opens visible band gaps so that the inside TSSs can be distinguished cushily, easy to observe in ARPES experiments, especially for YPb_3.

In conclusion, we have predicted three TS candidates of YIn_3, YTl_3, and YPb_3 by first-principles calculations. The superconductor YTl_3 is a topological type-II Dirac semimetal with 24 tilted DPs at boundary. The nontrivial topological invariants Z_2 are (0; 111) and (1; 111) for YIn_3 and YPb_3, respectively. The Rashba-like gapless TSSs and the Fermi arcs on (001) surface confirm our results. The intrinsic superconductivities are found using the framework of the BCS microscopic theory, proving that all these four systems are phonon-mediated superconductors. Based on our work, more materials of the $AuCu_3$-type structure could be explored for searching the semimetallic properties and Majorana fermions in experiment and theory, such as $LaSn_3$, $LaIn_3$, $LaTl_3$, and $LaPb_3$.

[1] S. Murakami, N. Nagaosa, and S.-C. Zhang, Dissipationless quantum spin current at room temperature, Science **301**, 1348 (2003).

[2] J. Sinova, D. Culcer, Q. Niu, N. A. Sinitsyn, T. Jungwirth, and A. H. MacDonald, Universal Intrinsic Spin Hall Effect, Phys. Rev. Lett. **92**, 126603 (2004).

[3] S. Murakami, N. Nagaosa, and S.-C. Zhang, Spin-Hall Insulator, Phys. Rev. Lett. **93**, 156804 (2004).

[4] M. König, S. Wiedmann, C. Brüne, A. Roth, H. Buhmann, L. W. Molenkamp, X.-L. Qi, and S.-C. Zhang, Quantum spin Hall insulator state in HgTe quantum wells, Science **318**, 766 (2007).

[5] H.-J. Zhang, C.-X. Liu, X.-L. Qi, X. Dai, Z. Fang, and S.-C. Zhang, Topological insulators in Bi_2Se_3, Bi_2Te_3, and Sb_2Te_3 with a single Dirac cone on the surface, Nat. Phys. **5**, 438 (2009).

[6] J. C. Y. Teo, L. Fu, and C. L. Kane, Surface states and topological invariants in three-dimensional topological insulators: Application to $Bi_{1-x}Sb_x$, Phys. Rev. B **78**, 045426 (2008).

[7] M. Z. Hasan and C. L. Kane, Colloquium: Topological insulators, Rev. Mod. Phys. **82**, 3045 (2010).

[8] A. Bansil, H. Lin, and T. Das, Colloquium: Topological band theory, Rev. Mod. Phys. **88**, 021004 (2016).

[9] X.-L. Qi and S.-C. Zhang, Topological insulators and superconductors, Rev. Mod. Phys. **83**, 1057 (2011).

[10] J. E. Moore, The birth of topological insulators, Nature (London) **464**, 194 (2010).

[11] P. Hořava, Stability of Fermi Surfaces and k Theory, Phys. Rev. Lett. **95**, 016405 (2005).

[12] H.-D. Song, D. Sheng, A.-Q. Wang, J.-G. Li, D.-P. Yu, and Z.-M. Liao, Topological transport in Dirac electronic systems: A concise review, Chin. Phys. B **26**, 037301 (2017).

[13] Z.-J. Wang, H.-M. Weng, Q.-S. Wu, X. Dai, and Z. Fang, Three-dimensional Dirac semimetal and quantum transport in Cd_3As_2, Phys. Rev. B **88**, 125427 (2013).

[14] H.-Z. Lu and S.-Q. Shen, Quantum transport in topological semimetals under magnetic fields, Front. Phys. **12**, 127201 (2017).

[15] T.-H. Liu, J.-W. Zhou, M.-D. Li, Z.-W. Ding, Q.-C. Song, B.-L. Liao, L. Fu, and G. Chen, Electron mean-free-path filtering in Dirac material for improved thermoelectric performance, Proc. Natl. Acad. Sci. USA **115**, 879 (2018).

[16] C. Nayak, S. H. Simon, A. Stern, M. Freedman, and S. D. Sarma, Non-Abelian anyons and topological quantum computation, Rev. Mod. Phys. **80**, 1083 (2008).

[17] M. Sato and Y. Ando, Topological superconductors: A review, Rep. Prog. Phys. **80**, 076501 (2017).

[18] J. D. Sau, R. M. Lutchyn, S. Tewari, and S. D. Sarma, Generic New Platform for Topological Quantum Computation Using Semiconductor Heterostructures, Phys. Rev. Lett. **104**, 040502 (2010).

[19] M. Freedman, A. Kitaev, M. Larsen, and Z.-h. Wang, Topological quantum computation, Bull. Am. Math. Soc. **40**, 31 (2003).

[20] Q.-S. Wu, C. Piveteau, Z. Song, and O. V. Yazyev, $MgTa_2N_3$: A reference Dirac semimetal, Phys. Rev. B **98**, 081115(R) (2018).

[21] R. Yu, H.-M. Weng, Z. Fang, X. Dai, and X. Hu, Topological Node-Line Semimetal and Dirac Semimetal State in Antiperovskite Cu_3PdN, Phys. Rev. Lett. **115**, 036807 (2015).

[22] Z.-K. Liu, J. Jiang, B. Zhou, Z.-J. Wang, Y. Zhang, H.-M. Weng, D. Prabhakaran, S. K. Mo, H. Peng, P. Dudin *et al.*, A stable three-dimensional topological Dirac semimetal Cd_3As_2, Nat. Mater. **13**, 677 (2014).

[23] Z.-K. Liu, B. Zhou, Y. Zhang, Z.-J. Wang, H.-M. Weng, D. Prabhakaran, S.-K. Mo, Z.-X. Shen, Z. Fang, X. Dai *et al.*, Discovery of a three-dimensional topological Dirac semimetal, Na_3Bi, Science **343**, 864 (2014).

[24] Z. Wang, D. Gresch, A. A. Soluyanov, W. Xie, S. Kushwaha, X. Dai, M. Troyer, R. J. Cava, and B. A. Bernevig, $MoTe_2$: A Type-II Weyl Topological Metal, Phys. Rev. Lett. **117**, 056805 (2016).

[25] H. Gao, Y. Kim, J. W. F. Venderbos, C. L. Kane, E. J. Mele, A. M. Rappe, and W. Ren, Dirac-Weyl Semimetal: Coexistence of Dirac and Weyl Fermions in Polar Hexagonal *ABC* Crystals, Phys. Rev. Lett. **121**, 106404 (2018).

[26] H.-M. Weng, C. Fang, Z. Fang, B. A. Bernevig, and X. Dai, Weyl Semimetal Phase in Noncentrosymmetric Transition-Metal Monophosphides, Phys. Rev. X **5**, 011029 (2015).

[27] H.-M. Weng, Y.-Y. Liang, Q.-N. Xu, R. Yu, Z. Fang, X. Dai, and Y. Kawazoe, Topological node-line semimetal in three-dimensional graphene networks, Phys. Rev. B **92**, 045108 (2015).

[28] Q.-N. Xu, R. Yu, Z. Fang, X. Dai, and H.-M. Weng, Topological nodal line semimetals in the CaP_3 family of materials, Phys. Rev. B **95**, 045136 (2017).

[29] P.-J. Chen, T.-R. Chang, and H.-T. Jeng, *Ab initio* study of the $PbTaSe_2$-related superconducting topological metals, Phys. Rev. B **94**, 165148 (2016).

[30] B.-T. Wang and E. R. Margine, Evolution of the topologically protected surface states in superconductor ß-Bi_2Pd from

the three-dimensional to the two-dimensional limit, J. Phys.: Condens. Matter **29**, 325501 (2017).
[31] X.-L. Qi, T. L. Hughes, S. Raghu, and S.-C. Zhang, Time-Reversal-Invariant Topological Superconductors and Superfluids in Two and Three Dimensions, Phys. Rev. Lett. **102**, 187001 (2009).
[32] L. Fu and E. Berg, Odd-Parity Topological Superconductors: Theory and Application to $Cu_xBi_2Se_3$, Phys. Rev. Lett. **105**, 097001 (2010).
[33] L. Fu and C. L. Kane, Superconducting Proximity Effect and Majorana Fermions at the Surface of a Topological Insulator, Phys. Rev. Lett. **100**, 096407 (2008).
[34] J.-F. Zhang, P.-J. Guo, M. Gao, K. Liu, and Z.-Y. Lu, β-$RhPb_2$: A topological superconductor candidate, Phys. Rev. B **99**, 045110 (2019).
[35] S. Kobayashi and M. Sato, Topological Superconductivity in Dirac Semimetals, Phys. Rev. Lett. **115**, 187001 (2015).
[36] T. Hashimoto, S. Kobayashi, Y. Tanaka, and M. Sato, Superconductivity in doped Dirac semimetals, Phys. Rev. B **94**, 014510 (2016).
[37] M. Alidoust, K. Halterman, and A. A. Zyuzin, Superconductivity in type-II Weyl semimetals, Phys. Rev. B **95**, 155124 (2017).
[38] L. Aggarwal, A. Gaurav, G. S. Thakur, Z. Haque, A. K. Ganguli, and G. Sheet, Unconventional superconductivity at mesoscopic point contacts on the 3D Dirac semimetal Cd_3As_2, Nat. Mater. **15**, 32 (2016).
[39] H.-J. Noh, J. Jeong, E.-J. Cho, K. Kim, B. I. Min, and B.-G. Park, Experimental Realization of Type-II Dirac Fermions in a $PdTe_2$ Superconductor, Phys. Rev. Lett. **119**, 016401 (2017).
[40] Y.-P. Qi, P. G Naumov, M. N Ali, C. R Rajamathi, W. Schnelle, O. Barkalov, M. Hanfland, S.-C. Wu, C. Shekhar, Y. Sun *et al.*, Superconductivity in Weyl semimetal candidate $MoTe_2$, Nat. Commun. **7**, 11038 (2016).
[41] E. E. Havinga, W-like dependence of critical temperature on number of valence electrons in non-transition metal Cu_3Au-type alloys, Phys. Lett. A **28**, 350 (1968).
[42] R. Szczęśniak, A. M. Duda, E. A. Drzazga, and M. A. Sowińska, The Eliashberg study of the electron-phonon superconductivity in YSn_3YSn_3 compound, Physica C **506**, 115 (2014).
[43] R. Sharma, G. Ahmed, and Y. Sharma, Intermediate coupled superconductivity in yttrium intermetallics, Physica C **540**, 1 (2017).
[44] S. Ram, V. Kanchana, G. Vaitheeswaran, A. Svane, S. B. Dugdale, and N. E. Christensen, Electronic topological transition in $LaSn_3$ under pressure, Phys. Rev. B **85**, 174531 (2012).
[45] H. Damsma and E. E. Havinga, Pressure dependence of superconductive transition temperatures in alloyed compounds $LaTl_{3-x}Pb_x$, Solid State Commun. **17**, 409 (1975).
[46] E. M. Bittar, C. Adriano, C. Giles, C. Rettori, Z. Fisk, and P. G. Pagliuso, Electron spin resonance study of the $LaIn_{3-x}Sn_x$ superconducting system, J. Phys.: Condens. Matter **23**, 455701 (2011).
[47] G. A. Costa, F. Canepa, and G. L. Olcese, Thermodynamic and magnetic properties of $LaSn_3$, Solid State Commun. **40**, 169 (1981).
[48] J. T. Demel, *Low Temperature Heat Capacity of YPb_3, $LaPb_3$, La_5Pb_3 and La_5Pb_3C* (Digital Repository @ Iowa State University, Iowa, 1973).
[49] K. Kawashima, M. Maruyama, M. Fukuma, and J. Akimitsu, Superconducting state in YSn_3 with a $AuCu_3$-type structure, Phys. Rev. B **82**, 094517 (2010).
[50] G. K. Shenoy, B. D. Dunlap, G. M. Kalvius, A. M. Tolffin, and R. J. Gambino, Magnetic and structural properties of some rare-earth-Sn_3 compounds, J. Appl. Phys. **41**, 1317 (1970).
[51] A. P. Murani, Magnetic spectral response in the intermetallic compound $CeSn_3$, Phys. Rev. B **28**, 2308 (1983).
[52] S. Ram, V. Kanchana, A. Svane, S. B. Dugdale, and N. E. Christensen, Fermi surface properties of AB_3 (A = Y, La; B = Pb, In, Tl) intermetallic compounds under pressure, J. Phys.: Condens. Matter **25**, 155501 (2013).
[53] J.-J. Cao, X.-F. Gou, and T.-G. Wang, Electron-phonon interaction and superconductivity in representative $AuCu_3$-type intermetallic compounds, Comput. Mater. Sci. **150**, 491 (2018).
[54] P. Giannozzi, S. Baroni, N. Bonini, M. Calandra, R. Car, C. Cavazzoni, D. Ceresoli, G. L. Chiarotti, M. Cococcioni, I. Dabo *et al.*, Quantum espresso: a modular and open-source software project for quantum simulations of materials, J. Phys.: Condens. Matter **21**, 395502 (2009).
[55] P. Hohenberg and W. Kohn, Inhomogeneous electron gas, Phys. Rev. **136**, B864 (1964).
[56] W. Kohn and L. J. Sham, Self-consistent equations including exchange and correlation effects, Phys. Rev. **140**, A1133 (1965).
[57] S. Baroni, S. De Gironcoli, A. Dal Corso, and P. Giannozzi, Phonons and related crystal properties from density-functional perturbation theory, Rev. Mod. Phys. **73**, 515 (2001).
[58] J. P. Perdew, K. Burke, and M. Ernzerhof, Generalized Gradient Approximation Made Simple, Phys. Rev. Lett. **77**, 3865 (1996).
[59] P. E. Blöchl, Projector augmented-wave method, Phys. Rev. B **50**, 17953 (1994).
[60] G. Kresse and D. Joubert, From ultrasoft pseudopotentials to the projector augmented-wave method, Phys. Rev. B **59**, 1758 (1999).
[61] E. E. Havinga, H. Damsma, and M. H. Van Maaren, Oscillatory dependence of superconductive critical temperature on number of valency electrons in Cu_3Au-type alloys, J. Phys. Chem. Solids **31**, 2653 (1970).
[62] B.-T. Wang, P. Zhang, R. Lizárraga, I. Di Marco, and O. Eriksson, Phonon spectrum, thermodynamic properties, and pressure-temperature phase diagram of uranium dioxide, Phys. Rev. B **88**, 104107 (2013).
[63] J.-J. Zheng and E. R. Margine, Electron-phonon coupling and pairing mechanism in β-Bi_2Pd centrosymmetric superconductor, Phys. Rev. B **95**, 014512 (2017).
[64] M.-J. Wei, W.-J. Lu, R.-C. Xiao, H.-Y. Lv, P. Tong, W.-H. Song, and Y.-P. Sun, Manipulating charge density wave order in monolayer 1t-$TiSe_2$ by strain and charge doping: A first-principles investigation, Phys. Rev. B **96**, 165404 (2017).
[65] L. Hou, W.-D. Li, F.-w. Wang, O. Eriksson, and B.-T. Wang, Structural, electronic, and thermodynamic properties of curium dioxide: Density functional theory calculations, Phys. Rev. B **96**, 235137 (2017).
[66] B.-T. Wang, P.-F. Liu, J.-J. Zheng, W. Yin, and F.-w. Wang, First-principles study of superconductivity in the two- and three-dimensional forms of $PbTiSe_2$: Suppressed charge density wave in 1t-$TiSe_2$, Phys. Rev. B **98**, 014514 (2018).

[67] Q.-S. Wu, S.-N. Zhang, H.-F. Song, M. Troyer, and A. A. Soluyanov, WannierTools: An open-source software package for novel topological materials, Comp. Phys. Commun. **224**, 405 (2018).

[68] P.-F. Liu, L.-J. Zhou, S. Tretiak, and L.-M. Wu, Two-dimensional hexagonal M_3C_2 (M = Zn, Cd, and Hg) monolayers: novel quantum spin Hall insulators and Dirac cone materials, J. Mater. Chem. C **5**, 9181 (2017).

[69] L. Fu, C. L. Kane, and E. J. Mele, Topological Insulators in Three Dimensions, Phys. Rev. Lett. **98**, 106803 (2007).

[70] L. Fu and C. L. Kane, Topological insulators with inversion symmetry, Phys. Rev. B **76**, 045302 (2007).

[71] M. Kargarian, M. Randeria, and Y.-M. Lu, Are the surface Fermi arcs in Dirac semimetals topologically protected?, Proc. Natl. Acad. Sci. USA **113**, 8648 (2016).

[72] See Supplemental Material at http://link.aps.org/supplemental/10.1103/PhysRevMaterials.3.054202 for our calculated phonon dispersions, phonon density of states, Eliashberg electron-phonon spectral function, EPC constants, and superconducting transition temperatures.

[73] Y. S. Hor, A. J. Williams, J. G. Checkelsky, P. Roushan, J. Seo, Q. Xu, H. W. Zandbergen, A. Yazdani, N. P. Ong, and R. J. Cava, Superconductivity in $Cu_xBi_2Se_3$ and its Implications for Pairing in the Undoped Topological Insulator, Phys. Rev. Lett. **104**, 057001 (2010).

[74] T. Asaba, B. J. Lawson, C. Tinsman, L. Chen, P. Corbae, G. Li, Y. Qiu, Y. S. Hor, L. Fu, and L. Li, Rotational Symmetry Breaking in a Trigonal Superconductor Nb-Doped Bi_2Se_3, Phys. Rev. X **7**, 011009 (2017).

[75] M. Novak, S. Sasaki, M. Kriener, K. Segawa, and Y. Ando, Unusual nature of fully gapped superconductivity in In-doped SnTe, Phys. Rev. B **88**, 140502(R) (2013).

[76] S.-M. Nie, L.-Y. Xing, R.-Y. Jin, W.-W. Xie, Z.-J. Wang, and F. B. Prinz, Topological phases in the $TaSe_3$ compound, Phys. Rev. B **98**, 125143 (2018).

[77] H. Leng, C. Paulsen, Y. K. Huang, and A. de Visser, Type-I superconductivity in the Dirac semimetal $PdTe_2$, Phys. Rev. B **96**, 220506(R) (2017).

[78] N. P. Butch, P. Syers, K. Kirshenbaum, A. P. Hope, and J. Paglione, Superconductivity in the topological semimetal YPtBi, Phys. Rev. B **84**, 220504(R) (2011).